ACS APPLIED MATERIALS & INTERFACES

Research Article

www.acsami.org

Lanthanum Aluminum Oxide Thin-Film Dielectrics from Aqueous Solution

Paul N. Plassmeyer,[†] Kevin Archila,[‡] John F. Wager,[‡] and Catherine J. Page*,[†]

[†]Department of Chemistry, University of Oregon, Eugene, Oregon 97403-1253, United States

[‡]School of EECS, Oregon State University, Corvallis, Oregon 97331-5501, United States

Supporting Information

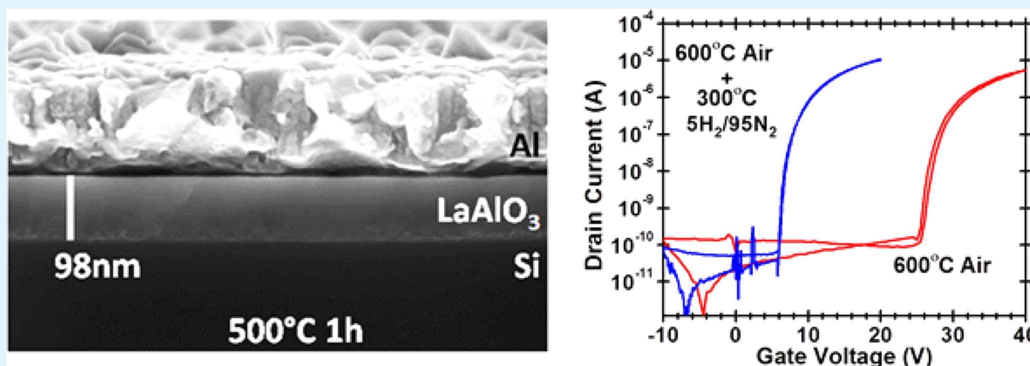

ABSTRACT: Amorphous $LaAlO_3$ dielectric thin films were fabricated via solution processing from inorganic nitrate precursors. Precursor solutions contained soluble oligomeric metal-hydroxyl and/or -oxo species as evidenced by dynamic light scattering (DLS) and Raman spectroscopy. Thin-film formation was characterized as a function of annealing temperature using Fourier transform infrared (FTIR), X-ray diffraction (XRD), X-ray reflectivity (XRR), scanning electron microscopy (SEM), and an array of electrical measurements. Annealing temperatures ≥500 °C result in thin films with low leakage-current densities (~1×10^{-8} $A \cdot cm^{-2}$) and dielectric constants ranging from 11.0 to 11.5. When incorporated as the gate dielectric layer in a-IGZO thin-film transistors (TFTs), $LaAlO_3$ thin films annealed at 600 °C in air yielded TFTs with relatively low average mobilities (~4.5 $cm^2 \cdot V^{-1} \cdot s^{-1}$) and high turn-on voltages (~26 V). Interestingly, reannealing the $LaAlO_3$ in $5\%H_2/95\%N_2$ at 300 °C before deposition of a-IGZO channel layers resulted in TFTs with increased average mobilities (11.1 $cm^2 \cdot V^{-1} \cdot s^{-1}$) and lower turn-on voltages (~6 V).

KEYWORDS: *aqueous solution process, thin-film transistor, metal-oxide, dielectric, lanthanum aluminum oxide*

INTRODUCTION

Rare earth aluminum oxides are of interest as scintillators and laser host materials,[1−4] as dielectric resonators,[5] as active components in nonvolatile memory elements,[6−9] and as high-dielectric gate oxides for thin film transistors.[10,11] For the latter applications, thin films are required. Where the rare earth element is lanthanum, crystalline and amorphous $LaAlO_3$ thin films have been widely studied as gate dielectrics in transistors,[12−14] as template layers for heteroepitaxial growth of high-T_c superconductors,[15,16] and for the intriguing electronic phenomena that arise at $LaAlO_3/SrTiO_3$ interfaces.[17]

A variety of techniques have been developed for the deposition of metal-oxide thin films.[18] Vapor deposition techniques such as atomic layer deposition (ALD), metal−organic chemical vapor depositions (MOCVD) and pulsed laser deposition (PLD) can yield thin films with excellent electronic and morphological properties, but stringent processing conditions and costly precursor materials are often required to obtain the desired film properties.[19−21] Much of the research directed toward thin-film $LaAlO_3$ has focused on deposition using such techniques.[22−30]

For applications tolerating higher defect levels and rougher topologies, solution deposition techniques, such as sol−gel, have been employed to make metal-oxide thin films.[15,16] However, the expulsion of bulky organic ligands during annealing tends to reduce the density and smoothness of films prepared in this way.[31] Deposition of $LaAlO_3$ has also been attempted using methanol solutions of nitrate salts.[32] Epitaxial growth of crystalline $LaAlO_3$ on $SrTiO_3$ substrates was achieved by this method, but the resultant films had large voids and irregular morphologies that would be problematic for electrical characterization or use in electronic devices.

In contrast to this previous report of crystalline $LaAlO_3$ films from methanol-based nitrate solutions, we report here the preparation of high-quality, ultrasmooth *amorphous* $LaAlO_3$

Received: October 20, 2014
Accepted: December 22, 2014
Published: December 22, 2014

© 2014 American Chemical Society

DOI: 10.1021/am507271e
ACS Appl. Mater. Interfaces 2015, 7, 1678−1684

films prepared from *aqueous* nitrate-containing solutions. Importantly, using this solution-based route, we are able to produce amorphous thin films that approach the quality normally associated with vapor deposition techniques. Our solution-phase approach to these materials employs inexpensive inorganic salts with small, easily decomposed counterions. By controlling the concentration, pH, and degree of condensation of solution-phase precursors, spun films can be heated quickly to promote prompt condensation to an oxide network.

The term 'Prompt Inorganic Condensation' (PIC) has been recently coined to describe this general approach, which has been used to produce a variety of metal oxide, metal oxide/phosphate, and metal oxide/sulfate films, including insulating films of $Al_2O_{3-3x}(PO_4)_{2x}$, HfO_2, $ZrO_{2-x}(SO_4)_x$, and $HfO_{2-x}(SO_4)_x$ and semiconducting ZnO and SnO_2.[33−38] Thicknesses of single layer films are typically in the 30−50 nm range for solutions that are 1 M in metal ion concentration, and overall film thickness can be adjusted by controlling solution concentration and the number of layers deposited. In the case of aluminum oxide and aluminum oxide phosphate, $Al_2O_{3-3x}(PO_4)_{2x}$, films produced using PIC have demonstrated relatively high dielectric breakdown voltages and low leakage currents.[33,39] When used as the insulating layer in thin-film transistors, high quality devices exhibiting small turn-on voltages with minimal hysteresis and high channel carrier mobility have been demonstrated.

For optimized condensation of metal-oxo networks using PIC, it is desirable to have "precondensed" solution-phase oxo- or hydroxo-bridged cluster species in the precursor solutions. In addition to being partially condensed, these species also have reduced positive charges and fewer counterions, which leads to increased atom-economy and less disruptive expulsion of ligands during film formation. Speciation of aluminum in aqueous solution is relatively well understood and can be controlled via concentration and solution pH. At low pH (≤1.5), isolated $Al(H_2O)_6^{3+}$ species dominate, but as pH is increased to ∼3.2 aluminum oxo-hydroxide clusters form.[40] The aqueous behavior of lanthanum is not unlike that of aluminum, although lanthanum is soluble to higher pH (∼7). No oxo- or hydroxyl-bridged lanthanum clusters have been isolated and characterized to date, although hexanuclear clusters with the general formula $[Ln_6O(OH)_8(NO_3)_6(H_2O)_{14}]^{2+}$ are known for other lanthanide ions.[41] It is possible that increasing the pH toward the solubility limit and/or removing counterions from a $La^{3+}{}_{(aq)}$ solution could produce similar oligomeric hydroxyl-bridged lanthanum species.

In this contribution, we report the PIC synthesis of high quality, amorphous $LaAlO_3$ thin films achieved by controlling precursor solution pH and reducing nitrate counterion concentration relative to solutions of metal nitrate salts. Dissolving La_2O_3 in $Al(NO_3)_{3(aq)}$ increases pH to levels where partial condensation of aluminum species is likely to occur (∼3.2) while reducing the nitrate anion to metal cation ratio. Moreover, the addition of highly polarizable lanthanum (La_2O_3 has a dielectric constant $K = 27$) increases the dielectric constant of the resulting thin films and suppresses crystallization. While we have focused exclusively on a 1:1 lanthanum aluminum oxide in this work, the synthetic route is broadly applicable to other stoichiometries and rare earth aluminum oxides.

EXPERIMENTAL SECTION

2.1. Solution Preparation. Typical $LaAlO_3$ thin-film precursor solutions were prepared by dissolving $Al(NO_3)_3{\cdot}9H_2O$ (18.757 g, 0.050 mol) in 80 mL of 18.2 MΩ·cm H_2O and adding ∼15.8 M $HNO_{3\,(aq)}$ (3.17 mL, 0.050 mol HNO_3). These solutions were heated to 70 °C and La_2O_3 (8.145 g, 0.025 mol) was added over 10 min while stirring. The solutions were then heated at 70 °C and stirred for an additional 3 h to ensure complete dissolution. Excessively high heating temperatures and/or times resulted in precipitation or gelation. After dissolution of La_2O_3, the solutions were diluted to 100 mL using 18.2 MΩ·cm H_2O. The resulting solutions were 0.5 M $Al(NO_3)_{3\,(aq)}$, 0.5 M $La^{3+}{}_{(aq)}$, 0.5 M HNO_3 with pH near 3.4.

2.2. Solution Characterization. Hydrodynamic radii of solution species were determined using a Möbius dynamic light scattering (DLS) model WMOB-03 using an acquisition time of 20 s. Correlation decays were modeled using a cumulant fit. Correlation curves and regularization fits can be found in Figure S1 (Supporting Information). Solution Raman spectra were collected using a Wytec 300S Raman spectrometer with laser power of 45 mW and excitation wavelength of 532 nm. Raman peak fits can be found in Figure S2 (Supporting Information). Thermogravimetric analyses were performed using a TA Instruments Q500 using a temperature ramp rate of 10 °C min^{-1} and ambient air.

2.3. Film Preparation. Moderate resistivity (∼45Ωcm) p-type and low resistivity (∼0.001 Ω·cm) n^+- or p^+-type Si were used as substrates for thin film deposition. Prior to deposition substrates were cleaned by sonication in a 5% Contrad 70 solution at 45 °C for 1 h. After thorough rinsing with 18.2 MΩ·cm H_2O, this procedure yielded a highly hydrophilic surface. Thin films were prepared by depositing precursor solutions onto the native oxide of Si substrates through 0.45 μm PTFE filters followed by rotation at 3000 rpm for 30 s. The wet films were then immediately soft-annealed at 100 °C on a hot-plate followed by a 12.5 °C min^{-1} ramp to a final target temperature between 200 and 700 °C. Solutions with 1 M total metal concentrations yielded films with a thickness of approximately 50 nm after a 300 °C anneal. Films used for electrical measurements (and thin-film transistors) were prepared by sequential deposition of three layers of slightly lower concentration (chosen to give a final total thickness of 100 nm), annealed to 300 °C between depositions, and then at the final annealing temperature for 1 h.

2.4. Thin-Film Characterization. Film thicknesses were determined by X-ray reflectivity (XRR) measurements on a Bruker D8 Discover diffractometer with a Cu Kα radiation source ($\lambda_{avg} = 1.5418$ Å). Analysis of reflectivity data was accomplished using Bede REFS software. Grazing-incidence X-ray diffraction experiments to determine film crystallinity (or lack thereof) were also performed on the Bruker D8 Discover diffractometer. Transmission IR measurements were performed on a Nicolet 6700 Fourier transform infrared (FTIR) spectrometer using a spectrum collected from a bare silicon substrate (45 Ω·cm) as the background. Electron probe microanalysis (EPMA) was performed using a Cameca SX-50. The resultant raw X-ray intensities were corrected as outlined by Donovan and Tingle.[42] Electron micrographs were obtained using a Zeiss Ultra-55 FESEM with a 20 μm aperture and 5 kV accelerating voltage.

2.5. Metal−Insulator−Semiconductor Device Fabrication. Metal−insulator−semiconductor (MIS) capacitors were constructed for impedance and current−voltage measurements by depositing 100 nm thick aluminum top contacts through a shadow mask onto annealed $LaAlO_3$ dielectric films deposited on Si substrates. This resulted in an array of MIS capacitors, each with an area of 0.011 cm^2. Potentials were always applied to the aluminum top contacts. Leakage current and dielectric strength measurements were performed on a Keithley 2400 source meter using a 50 mV step size and 50 ms delay. Impedance, phase-angle and capacitance−voltage measurements were conducted using a Hewlett-Packard 4284a impedance analyzer at 1 kHz with 50 mV oscillation amplitude.

2.6. Thin-Film Transistor Device Fabrication. Fabrication of thin-film transistors was performed on ∼100 nm thick $LaAlO_3$ thin films deposited on highly doped Si substrates annealed between 500

DOI: 10.1021/am507271e
ACS Appl. Mater. Interfaces 2015, 7, 1678−1684

and 700 °C in air for 1 h. After annealing in air, a subset of samples were annealed in 5%H_2/95%N_2 (forming gas) at 300 °C. Amorphous $InGaZnO_4$ (a-IGZO) semiconductor channels with dimensions W/L = 1000 μm/150 μm and thickness of 35 nm were sputter-deposited at a power of 75 W, gas flow of Ar/O_2 = 9/1 sccm, pressure of 5 mTorr and postdeposition anneal at 150 °C. Thermally evaporated Al was used for source/drain contacts. Transfer curves were measured on an Agilent 4155C semiconductor parameter analyzer.

RESULTS AND DISCUSSION

3.1. Solution Characterization. Use of La_2O_3 instead of $La(NO_3)_3$ as a source of lanthanum allows for the preparation of a precursor solution with a ratio of 4 NO_3^-:1 La^{3+}:1 Al^{3+} (i.e., a nitrate/metal ratio of 2:1) and a pH = 3.4, in contrast to a simple mixture of aluminum and lanthanum nitrate salts, for which the pH is significantly lower (1.6) and the nitrate/metal ratio is 3:1. Due to the low NO_3^-/M^{3+} ratio of our precursor solutions, monomeric or oligomeric metal-oxo or -hydroxyl species must exist in solution to achieve charge balance. DLS measurements indicate that there is an increase in the hydrodynamic radii of species in these solutions relative to those containing a mixture of nitrate salts, suggesting these species are oligomeric (Figure 1). It is thus likely that the hydroxide (or oxide) ligands serve as bridges between metal centers to give oligomeric species. We have attempted to isolate and identify these species without success. However, to distinguish the speciation in these solutions relative to those in solutions of nitrate salts, we will denote them as aqueous "LaAl oligomer " species throughout the remainder of the text.

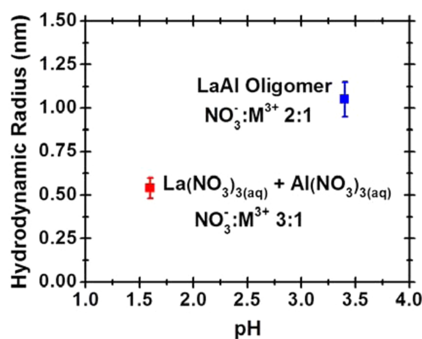

Figure 1. Dependence of hydrodynamic radius on solution pH and NO_3^-/M^{3+}.

The formation of oligomeric metal-hydroxyl/oxo species requires alterations to the inner hydration sphere of solvated metal cations as H_2O is replaced by OH^- or O^{2-}. In Figure 2 the Raman spectra of $Al(NO_3)_{3(aq)}$, $La(NO_3)_{3(aq)}$, $1La(NO_3)_3$/$1Al(NO_3)_{3(aq)}$, and "LaAl oligomer species" are compared to determine changes induced by increasing pH and reducing NO_3^- concentration. The reduced intensity of the $Al(OH_2)_6^{3+}$ modes at 530 and 340 cm^{-1} in "LaAl oligomer species" indicates that OH^- or O^{2-} may be substituting for H_2O in the inner sphere of Al^{3+},[43] although a weak shoulder attributable to the hydration sphere of La^{3+} still remains at ~350 cm^{-1}. The modes at 725 and 745 cm^{-1} arise from free NO_3^- and inner sphere NO_3^- bound to La^{3+}, respectively.[44−46] An overall decrease in the intensity of the free NO_3^- peak was observed in the "LaAl oligomer" solution as expected. The bound NO_3^- peak associated with La^{3+} remains essentially unchanged in the "LaAl oligomer" solution relative to that of lanthanum nitrate, which indicates that if lanthanum is incorporated into an oligomeric species it retains its coordinated nitrate ligand(s).

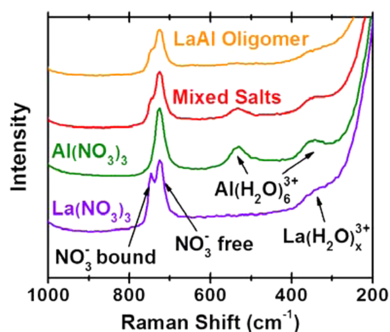

Figure 2. Raman spectra of $La(NO_3)_{3(aq)}$, $Al(NO_3)_{3(aq)}$, 1 $La(NO_3)_{3(aq)}$:1 $Al(NO_3)_{3(aq)}$ and "LaAl oligomer".

Upon deposition and subsequent annealing, condensation reactions occur between the remaining hydroxyl ligands while H_2O and NO_x gases are expelled. TGA experiments were performed on bulk powders of $La(NO_3)_3{\cdot}6H_2O$ and $Al(NO_3)_3{\cdot}9H_2O$, and dried powders obtained from solutions of "LaAl oligomer species" (Figure 3), to gain insight into the oxide formation process during annealing. For bulk $La(NO_3)_3{\cdot}6H_2O$, temperatures above 600 °C are required to remove a significant portion of water, hydroxides, and nitrate groups to yield La_2O_3. In contrast, most dehydration and counterion expulsion occurs by 300 °C for $Al(NO_3)_3{\cdot}9H_2O$. These results are not particularly surprising as it is known that the decomposition temperature of a given metal nitrate decreases as the metal ion charge density increases.[47] The high charge density of Al^{3+} draws electron density from the nitrate, effectively weakening the N−O bonds and making bond breakage associated with decomposition of the nitrate more facile. The large La^{3+} (~5 times the ionic volume of Al^{3+}) is less effective polarizing these bonds. Furthermore, NO_3^- coordinates in La^{3+} in a bidentate fashion, resulting in less N−O bond polarization.[46] TGA experiments on dried powders obtained from solutions containing "LaAl oligomer species" show that mass loss is essentially complete by 500 °C. This indicates that the presence of aluminum acts to decrease nitrate removal/decomposition temperature of the mixture relative to that required for $La(NO_3)_3{\cdot}6H_2O$. It should be noted these dried powders may not be truly representative of our rapidly dried films because sequential precipitation of salts may have occurred with the slower drying employed, but these results are consistent with the temperatures needed to expel nitrate from the films, as shown by IR and electrical data (see below).

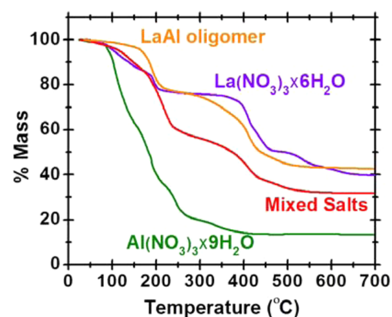

Figure 3. TGA curves of $La(NO_3)_3{\cdot}6H_2O(s)$, $Al(NO_3)_3{\cdot}9H_2O(s)$, and powders obtained by drying solutions of a mixture of the nitrate salts and of 1 La^{3+}:1 Al^{3+}:2 NO_3^- (denoted as "LaAl oligomer") in air.

DOI: 10.1021/am507271e
ACS Appl. Mater. Interfaces 2015, 7, 1678−1684

3.2. Thin Film Physical and Chemical Characterization. Residual H_2O and NO_x species have a significant impact on the properties of the thin films. To track the chemical processes during annealing, ex-situ infrared spectra of thin films were taken immediately after annealing at various temperatures (Figure 4). By monitoring the broad O−H stretching mode centered near 3500 cm^{-1} and the H−O−H bending mode at 1650 cm^{-1}, it can be seen that a significant portion of the water is lost between 200 and 300 °C. Disappearance of the H−O−H bending mode in this temperature range suggests low levels of H_2O, and the remaining OH absorption is predominately due to residual metal hydroxides. However, we note that films annealed below 250 °C are hygroscopic and the bands at 3500 and 1650 cm^{-1} grow if the films are exposed to ambient atmosphere. The OH absorption at 3500 cm^{-1} remains until annealing temperatures >400 °C, indicating that condensation is not complete until approximately 500 °C. The absorptions at 1280 and 1460 cm^{-1} correspond to residual nitrate trapped within the films.[44,45] Nitrate content also decreases throughout the annealing process, but it is still detectable even after annealing at 500 °C. The weak absorptions at 1040, 810, and 740 cm^{-1} present after annealing at only 200 °C are indicative of hydrated metal-nitrate species.[44,45] As annealing temperatures are increased, these absorptions are eliminated and a broad feature at 740 cm^{-1} appears. This absorption is related to the formation of metal−oxygen−metal bonds.[48]

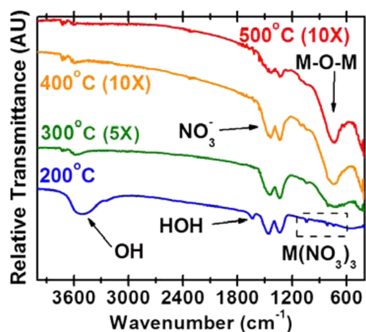

Figure 4. Fourier transform infrared (FTIR) spectra of thin films annealed between 200 and 500 °C in air.

XRR was employed to determine the thickness, roughness, and density of the thin films (Figure 5a). The hygroscopic instability of thin films annealed at temperatures <250 °C led to significant variations in the XRR, so these are not reported here. As annealing temperatures are increased from 300 to 600 °C, film thicknesses decrease by ≈35%, consistent with counterion expulsion and condensation. This is accompanied by a density increase from 61% to 72% of the single-crystal $LaAlO_3$ density of 6.51 g·cm^{-3}. These relative densities are similar to those attained by condensing Al_2O_3 thin films from similar conditions.[39] Cross-sectional and surface SEM micrographs reveal films with a high degree of uniformity and minimal surface and interfacial roughnesses (Figure 5b). Thin films crystallize between 800 and 900 °C to the rhombohedral perovskite phase (JCPDS File Card No. 31-22) (Figure 5c).

3.3. Thin Film Electrical Characterization. Dielectric breakdown and leakage current characteristics were examined by performing current−voltage measurements on MIS capacitors consisting of thin $LaAlO_3$ films sandwiched between highly doped n-type Si substrates and aluminum top contacts

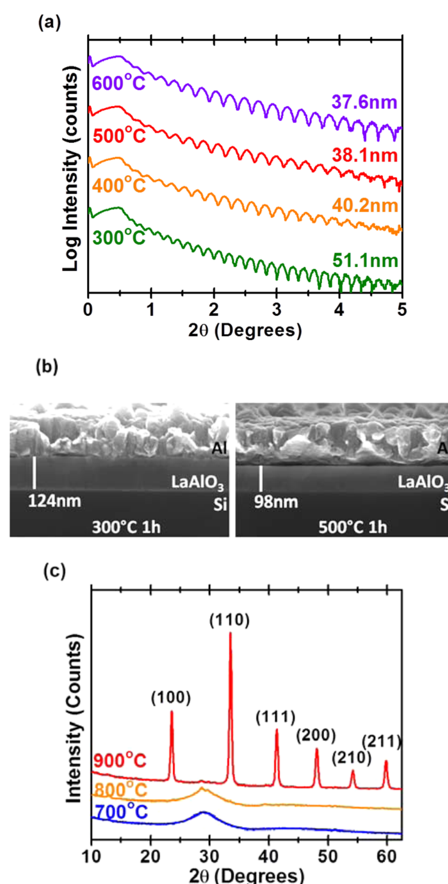

Figure 5. (a) XRR patterns of $LaAlO_3$ thin films annealed between 300 and 600 °C, (b) SEM micrographs of $LaAlO_3$ thin films annealed at 300 and 500 °C, (c) X-ray diffraction (XRD) patterns of $LaAlO_3$ thin films annealed at 700, 800, and 900 °C. The 900 °C pattern is indexed as the rhombohedral perovskite $LaAlO_3$ phase.

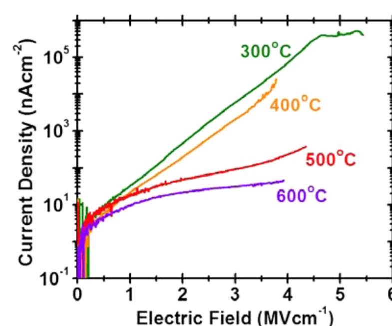

Figure 6. Current density as a function of electric field applied through 100 nm thick $LaAlO_3$ thin films annealed between 300 and 600 °C in air.

(Figure 6). Leakage currents are high for films annealed at temperatures ≤400 °C, likely related to defects associated with incomplete condensation. Catastrophic breakdown generally occurs at electric fields >3.5 MV·cm^{-1}. Leakage current profiles decrease in slope with increasing annealing temperature, suggesting a reduction in electronic defects. This reduction is most likely associated with removal of counterions and residual hydration and is consistent with the TGA and IR data.

Dielectric constants and loss tangents of the films are shown in Figure 7a. The dielectric constant decreases as annealing temperatures are increased from 300 to 450 °C and then

DOI: 10.1021/am507271e
ACS Appl. Mater. Interfaces 2015, 7, 1678−1684

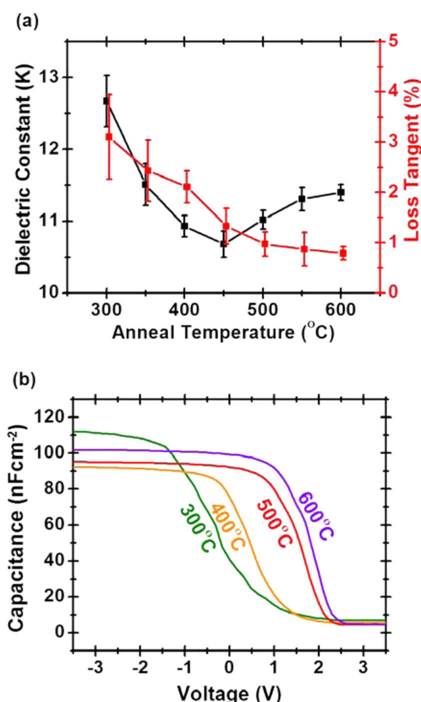

Figure 7. Dielectric constant (a) and capacitance–voltage curves (b) of $LaAlO_3$ thin films annealed between 300 and 600 °C.

increases slightly for samples annealed above 450 °C. The loss tangent, which is related to current passage, decreases with increasing annealing temperatures up to 500 °C and then levels off. We attribute the trends between 300 and 450 °C to removal of water, hydroxides, and nitrates, reducing the amount of mobile charged species in the films. The presence of mobile charged species also contributes to the overall polarizability (and thereby the dielectric constant) of the material. Above 450 °C, most of the mobile ions have been removed (hence the relatively constant loss tangent), so the dielectric constant increase for films annealed above 450 °C can be attributed to densification of the remaining metal-oxide framework.

Capacitance–voltage measurements reveal that higher annealing temperatures result in an increased flatband potential (Figure 7b). Generally, a positive (negative) shift in the flatband voltage indicates the presence of a negative (positive) fixed charge in the oxide near the semiconductor interface.[49] When in contact with SiO_2, most metal oxides, including La_2O_3, have positive fixed charge at this interface, which results in a negative flatband shift. However, positive shifts in flatband voltages in photovoltaics are well documented for recombination-passivating Al_2O_3/SiO_2 interfaces. At these interfaces, tetrahedrally coordinated Al centers possess a partial negative charge, pushing electrons away from the interface and shifting the flatband potentials toward positive values.[50,51] Assuming that the observed flatband shifts originate from fixed charges near this interface, the fixed charge density, Q_f, can be expressed as

$$Q_f = -C_I \Delta V_{fb} \quad (1)$$

where C_I is the insulator capacitance density and ΔV_{fb} is the difference between the observed and expected flatband voltages. The calculated interface charge densities at the $LaAlO_3/SiO_2$ interface range from $+1.45 \times 10^{11}$ cm^{-2} for films annealed at 300 °C to -1.75×10^{12} cm^{-2} for films annealed at 600 °C. The values calculated for films annealed at 600 °C match well with values from Al_2O_3 films deposited on the oxide of p-Si described in the literature.[50,51] We postulate that Al may preferentially bind to the native SiO_2 layer and create a similar interfacial charge in $LaAlO_3$ films deposited via PIC.

3.4. Thin-Film Transistor Characterization. To investigate the performance of these amorphous $LaAlO_3$ films in thin-film transistors, devices were fabricated by sputter depositing a-IGZO channels, with L = 150 μm and W = 1000 μm, and Al source/drain contacts on solution-processed $LaAlO_3$ deposited on p^+-Si (annealed at 600 °C in air). Although the characteristics of the capacitance–voltage data shown in Figure 7b suggest the presence of *some* inhomogeneous charge distribution and charge trapping defects at the $LaAlO_3/SiO_2$ interface, these thin-film transistors indicate there is a *large* concentration of empty electronic traps at the a-IGZO/$LaAlO_3$ interface, indicated by high turn-on voltages (≥24 V), moderate drain-current hysteresis and relatively low average mobilities of ~4.5 $cm^2 \cdot V^{-1} \cdot s^{-1}$ (Figure 8). Similar

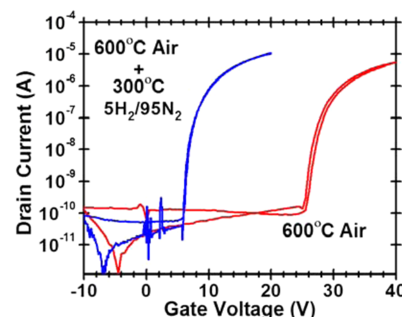

Figure 8. Transfer curves for bottom-gate TFTs with $LaAlO_3$ gate and sputtered IGZO channels. $LaAlO_3$ gates were annealed at 600 °C in air or at 600 °C in air followed by 300 °C in 5%H_2/95%N_2.

results have been found for IGZO transistors that incorporate a $LaAlO_3$ dielectric in direct contact with the IGZO channel.[52] Typically, the performance of such transistors has been improved by incorporating a passivating dielectric layer between the IGZO channel and the $LaAlO_3$ dielectric.[13,14,52] In this work, we employed an alternative "surface passivation" achieved by a second annealing at 300 °C in 5%H_2/95%N_2 (forming gas) after initial preparation of the $LaAlO_3$ thin film but prior to a-IGZO deposition. Surface passivation drastically lowered the turn-on voltage to ~6 V, minimized drain-current hysteresis, and increased average mobility to ~11.1 $cm^2 \cdot V^{-1} \cdot s^{-1}$ (Figure 8). According to the discrete donor trap model the turn-on voltage, V_{ON}, is given by

$$V_{ON} = \frac{-q}{C_I}(n_{co} - p_{to}) \quad (2)$$

where q is the electronic charge, C_I is the insulator capacitance density, n_{co} is the free electron sheet density, and p_{to} is the empty trap sheet density.[53] From this relationship, a turn-on voltage of 26 V corresponds to an empty trap sheet density of 1.7×10^{13} cm^{-2}, whereas a turn-on voltage of 6 V corresponds to a trap sheet density of 3.8×10^{12} cm^{-2}. Thus, the surface passivation anneal significantly reduces the empty trap sheet density. Although the detailed nature of the chemical origin of this dramatic reduction in the empty trap density is unknown at present, it (i) is clearly associated with the insulator, rather than the semiconductor, since the semiconductor is deposited

DOI: 10.1021/am507271e
ACS Appl. Mater. Interfaces 2015, 7, 1678–1684

subsequent to annealing, and (ii) is likely due to the removal of moisture and/or impurities in the $LaAlO_3$ film since the surface passivation anneal is performed in a reducing ambient.

CONCLUSIONS

The formation and properties of $LaAlO_3$ thin films deposited on Si using a 'prompt inorganic condensation' (PIC) process have been examined. In contrast to using a precursor solution of aluminum and lanthanum nitrates, dissolution of $La_2O_{3(s)}$ into $Al(NO_3)_{3(aq)}$ results in an increased solution pH, a lower nitrate/metal ratio and the formation of oligomeric hydroxyl- or oxo-metal species, which are postulated to aid in the condensation of the metal-oxide network upon annealing. Thermogravimetric analysis (TGA) and IR data suggest essentially complete condensation, dehydration, and counterion expulsion by 500 °C. X-ray reflectivity (XRR) and scanning electron microscopy (SEM) indicate very uniform films with low surface and interfacial roughness. Temperatures above 400 °C are required to achieve low leakage currents and expel the remaining mobile species, which likely contribute to the higher dielectric constants at lower annealing temperatures. Capacitance−voltage measurements indicate the presence of trapped negative charge near the $LaAlO_3/SiO_2$ interface, most notably at higher annealing temperatures. The trapped charge in the $LaAlO_3$ thin film could be useful for surface-recombination passivation in p-type emitter solar cells.

TFTs with sputtered a-IGZO channels were fabricated with PIC-deposited $LaAlO_3$ gate dielectrics. For $LaAlO_3$ gates annealed in air at 600 °C, large turn-on voltages, large drain-current hystereses, and relatively small average mobilities were observed. A low temperature post anneal step of the $LaAlO_3$ gate in reducing atmosphere decreased turn-on voltages and drain-current hystereses while increasing average mobility. This interesting result indicates a promising future direction for improving the electrical properties of these films to make them attractive candidates as dielectrics in thin-film transistors.

ASSOCIATED CONTENT

Supporting Information

DLS correlation curves/regularization fits and Raman peak fitting. This material is available free of charge via the Internet at http://pubs.acs.org.

AUTHOR INFORMATION

Corresponding Author

*E-mail: cpage@uoregon.edu.

Author Contributions

The manuscript was written through contributions of all authors. All authors have given approval to the final version of the manuscript.

Notes

The authors declare no competing financial interest.

ACKNOWLEDGMENTS

The authors thank Kurt Langworthy and John Donovan for assistance with SEM imaging and EPMA, respectively. We thank Milton Jackson for assistance with Raman spectroscopy and DLS measurements. We thank Christopher Knutson for helpful discussions. This research was supported by the National Science Foundation through CCI Grant CHE-1102637.

REFERENCES

(1) Duan, C.; Tanner, P.; Makhov, V.; Kirm, M. Vacuum Ultraviolet Spectra and Crystal Field Analysis of $YAlO_3$ Doped with Nd^{3+} and Er^{3+}. *Phys. Rev. B* **2007**, *75*, 195130 1−12.

(2) Stanek, C. R.; McClellan, K. J.; Levy, M. R.; Grimes, R. W. Defect Behavior in Rare Earth $REAlO_3$ Scintillators. *J. Appl. Phys.* **2006**, *99*, 113518 1−7.

(3) Gruber, J. B.; Nash, K. L.; Yow, R. M.; Sardar, D. K.; Valiev, U. V.; Uzokov, A. A.; Burdick, G. W. Spectroscopic and Magnetic Susceptibility Analyses of the ^7F_J and $^5D_4$ Energy Levels of $Tb^{3+}(4f^8)$ in $TbAlO_3$. *J. Lumin.* **2008**, *128*, 1271−1284.

(4) Weber, J. K. R.; Abadie, J. G.; Key, T. S.; Hiera, K.; Nordine, P. C. Synthesis and Optical Properties of Rare-Earth−Aluminum Oxide Glasses. *J. Am. Ceram. Soc.* **2002**, *11*, 1309−1311.

(5) Cho, S. Y.; Kim, I. T.; Hong, K. S. Microwave Dielectric Properties and Applications of Rare-Earth Aluminates. *J. Mater. Res.* **1999**, *14*, 114−119.

(6) Suhane, A.; Cacciato, A.; Richard, O.; Arreghini, A.; Adelmann, C.; Swerts, J.; Rothschild, O.; Van den bosch, G.; Breuil, L.; Bender, H.; Jurczak, M.; Debusschere, I.; Kittl, J. A.; De Meyer, K.; Van Houdt, J. Rare-Earth Aluminates as a Charge Trapping Materials for NAND Flash Memories: Integration and Electrical Evaluation. *Solid-State Electron.* **2011**, *65−66*, 177−183.

(7) Wu, S. X.; Peng, H. Y.; Wu, T. Concurrent Nonvolatile Resistance and Capacitance Switching in $LaAlO_3$. *Appl. Phys. Lett.* **2011**, *98*, 093503 1−3.

(8) Zahid, M. B.; Degraeve, R.; Toledano-Luque, M.; Van Houdt, J. Characterization of Hexagonal Rare-Earth Aluminates for Application in Flash Memories. *IEEE Int. Reliab. Phys. Symp. Proc.* **2011**, 815−818.

(9) Zhao, C.; Zhao, C. Z.; Lu, Q.; Yan, X.; Taylor, S.; Chalker, P. R. Hysteresis in Lanthanide Aluminum Oxides Observed by Fast Pulse CV Measurement. *Materials* **2014**, *7*, 6965−6981.

(10) Leskelä, M.; Kukli, K.; Ritala, M. Rare-Earth Oxide Thin Films for Gate Dielectrics in Microelectronics. *J. Alloys Compd.* **2006**, *418*, 27−34.

(11) Lopes, J. M. J.; Roeckerath, M.; Heeg, T.; Littmark, U.; Schubert, J.; Mantl, S.; Jia, Y.; Schlom, D. G. La-Based Ternary Rare-Earth Oxides as Alternative High-κ Dielectrics. *Microelectron. Eng.* **2007**, *84*, 1890−1893.

(12) Bere, M. K.; Liu, Y.; Kyaw, L. M.; Ngoo, Y. J.; Singh, S. P.; Chor, E. F. Fabrication and Performances of InAlN/GaN-on-Si MOSHEMTs with $LaAlO_3$ Gate Dielectric Using Gate-First CMOS Compatible Process at Low Thermal Budget. *ECS Trans.* **2014**, *61*, 271−280.

(13) Wu, C. H.; Wang, S. J.; Huang, H. Y.; Chang, K. M.; Hsu, H. Y. Investigation of $LaAlO_3/ZrO_2$/a-InGaZnO Thin-Film Transistors Using Atmospheric Pressure Plasma Jet. *Electron. Lett.* **2014**, *50*, 706−708.

(14) Zheng, Z. W.; Cheng, C. H.; Chen, Y. C. Low Operation Voltage InGaZnO Thin Film Transistors with $LaAlO_3$ Gate Dielectric Incorporation. *ECS J. Solid State Sci. Technol.* **2013**, *2*, 179−181.

(15) Shoup, S. S.; Paranthaman, M.; Beach, D. B.; Specht, E. D.; Williams, R. K. Sol-gel Synthesis of $LaAlO_3$; Epitaxial Growth of $LaAlO_3$ Thin Films on $SrTiO_3$ (100). *J. Mater. Res.* **1997**, *12*, 1017−1021.

(16) Shoup, S. S.; Paranthaman, M.; Goyal, A.; Specht, E. D.; Lee, D. F.; Kroeger, D. M.; Beach, D. B. Epitaxial Thin Film Growth of Lanthanum and Neodymium Aluminate Films on Roll-Textured Nickel Using a Sol-Gel Method. *J. Am. Ceram. Soc.* **1998**, *81*, 3019−3021.

(17) Huijben, M.; Brinkman, A.; Koster, G.; Rijnders, G.; Hilgenkamp, H.; Blank, D. H. A. Structure−Property Relation of $SrTiO_3/LaAlO_3$ Interfaces. *Adv. Mater.* **2009**, *21*, 1665−1677.

(18) Fortunato, E.; Barquinha, P.; Martins, R. Oxide Semiconductor Thin-Film Transistors: A Review of Recent Advances. *Adv. Mater.* **2012**, *24*, 2945−2986.

(19) Niinisto, L.; Nieminen, M.; Paivasaari, J.; Niinisto, J.; Putkonen, M.; Nieminen, M. Advanced Electronic and Optoelectronic Materials by Atomic Layer Deposition: An Overview with Special Emphasis on

Recent Progress in Processing of High-K Dielectrics and Other Oxide Materials. *Phys. Status Solidi A* **2004**, *201*, 1443−1452.

(20) Jones, A. C.; Chalker, P. R. Some Recent Developments in the Chemical Vapor Deposition of Electroceramic Oxides. *J. Phys. D: Appl. Phys.* **2003**, *36*, 80−95.

(21) Christen, H. M.; Eres, G. Recent Advances in Pulsed-Laser Deposition of Complex Oxides. *J. Phys.: Condens. Matter* **2008**, *20*, 264005 1−16.

(22) Jia, T. T.; Cheng, X. H.; Chao, D.; Xu, D. W.; Wang, Z. J.; Xia, C.; Zhang, Y. W.; Yu, Y. H. Properties of $LaAlO_3$ Thin Film on GaAs(100) Treated by In Situ NH_3 Plasma. *Nucl. Instrum. Methods Phys. Res, Sect B* **2013**, *307*, 349−352.

(23) Liu, K. C.; Tzeng, W. H.; Chang, K. M.; Huang, J. J.; Lee, Y. J.; Yeh, P. H.; Chen, P. S.; Lee, H. Y.; Chen, F.; Tsai, M. J. Investigation of the Effect of Different Oxygen Partial Pressure to $LaAlO_3$ Thin Film Properties and Resistive Switching Characteristics. *Thin Solid Films* **2011**, *520*, 1246−1250.

(24) Wu, S.; Ren, L.; Qing, J.; Yu, F.; Yang, K.; Yang, M.; Wang, Y.; Meng, M.; Zhou, W.; Zhou, X.; Li, S. Bipolar Resistance Switching in Transparent $ITO/LaAlO_3/SrTiO_3$ Memristors. *ACS Appl. Mater. Interfaces* **2014**, *6*, 8575−8579.

(25) Lu, X. B.; Liu, Z. G.; Zhang, X.; Huang, R.; Zhou, H. W.; Wang, X. P.; Nguyen, B. C. Investigation of High-Quality Ultra-Thin $LaAlO_3$ Films as High-κ Gate Dielectrics. *J. Phys. D: Appl. Phys.* **2003**, *36*, 3047−3050.

(26) Vellianitis, G.; Apostolopoulos, G.; Mavrou, G.; Argyropoulos, K.; Dimoulas, A.; Hooker, J. C.; Conard, T.; Butcher, M. MBE Lanthanum-Based High-K Gate Dielectrics as Candidates for SiO_2 Gate Oxide Replacement. *Mater. Sci. Eng., B* **2004**, *109*, 85−88.

(27) Li, A. D.; Shao, Q. Y.; Ling, H. Q.; Cheng, J. B.; Wu, D.; Liu, Z. G.; Ming, N. B.; Wang, C.; Zhou, H. W.; Nguyen, B. Y. Characteristics of $LaAlO_3$ Gate Dielectrics on Si Grown by Metalorganic Chemical Vapor Deposition. *Appl. Phys. Lett.* **2003**, *83*, 3540−3542.

(28) Lu, X.; Liu, Z.; Wang, Y.; Yang, Y.; Wang, X.; Zhou, H.; Nguyen, B. Structure and Dielectric Properties of Amorphous $LaAlO_3$ and $LaAlO_xN_y$ Films as Alternative Gate Dielectric Materials. *J. Appl. Phys.* **2003**, *94*, 1229−1234.

(29) Xiang, W.; Lü, H.; Yan, L.; Guo, H.; Liu, L.; Zhou, Y.; Yang, G.; Jiang, J.; Cheng, H.; Chen, Z. Characteristics of $LaAlO_3$/Si (100) Deposited under Various Oxygen Pressures. *J. Appl. Phys.* **2003**, *93*, 533−536.

(30) Chang, I. Y.; You, S.; Juan, P.; Wang, M.; Lee, J. Y. The Electrical and Interfacial Properties of Metal-High-κ Oxide Semiconductor Field-Effect Transistors With $LaAlO_3$ Gate Dielectric. *IEEE Electron Device Lett.* **2009**, *30*, 161−164.

(31) Chung, W. F.; Chang, T. C.; Li, H. W.; Chen, S. C.; Chen, Y. C.; Tseng, T. Y.; Tai, Y. H. Environment-Dependent Thermal Instability of Sol-Gel Derived Amorphous Indium-Gallium-Zinc-Oxide Thin Film Transistors. *Appl. Phys. Lett.* **2011**, *98*, 152109 1−3.

(32) Ng, M. F.; Cima, M. J. Heteroepitaxial Growth of Lanthanum Aluminate Films Derived from Mixed Metal Nitrates. *J. Mater. Res.* **1997**, *12*, 1306−1314.

(33) Meyers, S. T.; Anderson, J. T.; Hong, D.; Hung, C. M.; Wager, J. F.; Keszler, D. A. Solution-Processed Aluminum Oxide Phosphate Thin-Film Dielectrics. *Chem. Mater.* **2007**, *19*, 4023−4029.

(34) Jiang, K.; Anderson, J. T.; Hoshino, K.; Li, D.; Wager, J. F.; Keszler, D. A. Low-Energy Path to Dense HfO_2 Thin Films with Aqueous Precursor. *Chem. Mater.* **2011**, *23*, 945−952.

(35) Anderson, J. T.; Munsee, C. L.; Hung, C. M.; Phung, T. M.; Herman, G. S.; Johnson, D. C.; Wager, J. F.; Keszler, D. A. Solution-Processed HafSOx and ZircSOx Inorganic Thin-Film Dielectrics and Nanolaminates. *Adv. Funct. Mater.* **2007**, *17*, 2117−2124.

(36) Park, S. Y.; Kim, B. J.; Kim, K.; Kang, M. S.; Lim, K. H.; Lee, T. I; Myoung, J. M.; Baik, H. K.; Cho, J. H.; Kim, Y. S. Low-Temperature, Solution-Processed and Alkali Metal Doped ZnO for High-Performance Thin-Film Transistors. *Adv. Mater.* **2012**, *24*, 834−838.

(37) Meyers, S. T.; Anderson, J. T.; Hung, C. M.; Thompson, J.; Wager, J. F.; Keszler, D. A. Aqueous Inorganic Inks for Low-Temperature Fabrication of ZnO TFTs. *J. Am. Chem. Soc.* **2008**, *130*, 17603−17609.

(38) Nadarajah, A.; Carnes, M. E.; Kast, M. G.; Johnson, D. W.; Boettcher, S. W. Aqueous Solution Processing of F-Doped SnO_2 Transparent Conducting Oxide Films Using a Reactive Tin(II) Hydroxide Nitrate Nanoscale Cluster. *Chem. Mater.* **2013**, *25*, 4080−4087.

(39) Smith, S. W.; Wang, W.; Keszler, D. A.; Conley, J. F. Solution Based Prompt Inorganic Condensation and Atomic Layer Deposition of Al_2O_3 Films: A Side-by-Side Comparison. *J. Vac. Sci. Technol., A* **2014**, *32*, 041501 1−7.

(40) Wang, W.; Wentz, K. M.; Hayes, S. E.; Johnson, D. W.; Keszler, D. A. Synthesis of the Hydroxide Cluster $[Al_{13}(\mu_3\text{-}OH)_6(\mu\text{-}OH)_{18}(H_2O)_{24}]^{15+}$ From an Aqueous Solution. *Inorg. Chem.* **2011**, *50*, 4683−4685.

(41) Calvez, G.; Daiguebonne, C.; Guillou, O.; Le Dret, F. A New Series of Anhydrous Lanthanide-Based Octahedral Hexanuclear Complexes. *Eur. J. Inorg. Chem.* **2009**, 3172−3178.

(42) Donovan, J.; Tingle, T. An Improved Mean Atomic Number Background Correction for Quantitative Microanalysis. *J. Microsc. Soc. Am.* **1996**, 1−7.

(43) Rudolph, W. W.; Mason, R.; Pye, C. C. Aluminium(III) Hydration in Aqueous Solution. A Raman Spectroscopic Investigation and an Ab Initio Molecular Orbital Study of Aluminium(III) Water Clusters. *Phys. Chem. Chem. Phys.* **2000**, *2*, 5030−5040.

(44) Knoeckl, J. Vibrational Spectrometric and Electrochemical Lanthanum(III)-Nitrate Complexes in Aqueous. *Anal. Chem.* **1969**, *41*, 2069−2071.

(45) Kanno, H.; Hiraishi, J. Raman Study of Aqueous Rare-Earth Nitrate Solutions in Liquid and Glassy States. *J. Phys. Chem.* **1984**, *88*, 2787−2792.

(46) Klingenberg, B.; Vannice, M. A. Influence of Pretreatment on Lanthanum Nitrate, Carbonate, and Oxide Powders. *Chem. Mater.* **1996**, *8*, 2755−2768.

(47) Yuvaraj, S.; Fan-Yuan, L.; Tsong-Huei, C.; Chuin-Tih, Y. Thermal Decomposition of Metal Nitrates in Air and Hydrogen Environments. *J. Phys. Chem. B* **2003**, *107*, 1044−1047.

(48) Devine, R. A. B. Infrared and Electrical Properties of Amorphous Sputtered $(La_xAl_{1-x})_2O_3$ Films. *J. Appl. Phys.* **2003**, *93*, 9938−9942.

(49) Sze, S. M.; Ng, K. K. *Physics of Semiconductor Devices*, 3rd ed; Wiley-Interscience: Hoboken, NJ, 2007; pp 223−225.

(50) Schmidt, J.; Merkle, A.; Brendel, R.; Hoex, B.; van de Sanden, M. C. M.; Kessels, W. M. M. Surface Passivation of High-Efficiency Silicon Solar Cells by Atomic-Layer-Deposited Al_2O_3. *Prog. Photovoltaics* **2008**, *16*, 461−466.

(51) Hoex, B.; Schmidt, J.; Bock, R.; Altermatt, P. P.; van de Sanden, M. C. M.; Kessels, W. M. M. Excellent Passivation of Highly Doped P-Type Si Surfaces by the Negative-Charge-Dielectric Al_2O_3. *Appl. Phys. Lett.* **2007**, *91*, 112107 1−3.

(52) Zheng, Z. W.; Chen, Y. C. Improved Performances in Low-Voltage-Driven InGaZnO Thin Film Transistors Using a SiO_2 Buffer Layer Insertion. *Appl. Phys. A: Mater. Sci. Process.* **2014**, *115*, 937−941.

(53) Wager, J. F.; Keszler, D. A.; Presley, R. E. *Transparent Electronics*; Springer: New York, 2008; pp 234−238.

DOI: 10.1021/am507271e
ACS Appl. Mater. Interfaces 2015, 7, 1678−1684